International Journal of Extreme Manufacturing

PAPER • **OPEN ACCESS**

Electric-driven flexible-roller nanoimprint lithography on the stress-sensitive warped wafer

To cite this article: Yu Fan *et al* 2023 *Int. J. Extrem. Manuf.* **5** 035101

View the article online for updates and enhancements.

You may also like

- A template bank to search for gravitational waves from inspiralling compact binaries: II. Phenomenological model
  T Cokelaer
- ON THE CONSTRUCTION OF A NEW STELLAR CLASSIFICATION TEMPLATE LIBRARY FOR THE LAMOST SPECTRAL ANALYSIS PIPELINE
  Peng Wei, Ali Luo, Yinbi Li et al.
- Multi-Metallic Template Fluorination Mmtf for the Preparation of Ternary Metal Fluoride and Their First Use As Cathodes in Solid State Lithium Batteries
  Fabien Eveillard, Fabrice Leroux, Nicolas Batisse et al.

This content was downloaded from IP address 170.178.169.102 on 02/06/2023 at 10:07

OPEN ACCESS
IOP Publishing | IMMT
International Journal of Extreme Manufacturing
Int. J. Extrem. Manuf. **5** (2023) 035101 (11pp)
https://doi.org/10.1088/2631-7990/acd827

Electric-driven flexible-roller nanoimprint lithography on the stress-sensitive warped wafer

Yu Fan[1,2], Chunhui Wang[1,*], Jiaxing Sun[1], Xiaogang Peng[1], Hongmiao Tian[1], Xiangming Li[1,2], Xiaoliang Chen[1,2], Xiaoming Chen[1] and Jinyou Shao[1,2,*]

[1] Micro- and Nano-technology Research Center, State Key Laboratory for Manufacturing Systems Engineering, Xi'an Jiaotong University, Xi'an 710049, People's Republic of China
[2] Frontier Institute of Science and Technology (FIST), Xi'an Jiaotong University, Xi'an 710049, People's Republic of China

E-mail: chw-nanoman@xjtu.edu.cn and jyshao@xjtu.edu.cn

Received 13 January 2023, revised 27 March 2023
Accepted for publication 23 May 2023
Published 2 June 2023

Abstract

Surface nanopatterning of semiconductor optoelectronic devices is a powerful way to improve their quality and performance. However, photoelectric devices' inherent stress sensitivity and inevitable warpage pose a huge challenge on fabricating nanostructures large-scale. Electric-driven flexible-roller nanoimprint lithography for nanopatterning the optoelectronic wafer is proposed in this study. The flexible nanoimprint template twining around a roller is continuously released and recovered, controlled by the roller's simple motion. The electric field applied to the template and substrate provides the driving force. The contact line of the template and the substrate gradually moves with the roller to enable scanning and adapting to the entire warped substrate, under the electric field. In addition, the driving force generated from electric field is applied to the surface of substrate, so that the substrate is free from external pressure. Furthermore, liquid resist completely fills in microcavities on the template by powerful electric field force, to ensure the fidelity of the nanostructures. The proposed nanoimprint technology is validated on the prototype. Finally, nano-grating structures are fabricated on a gallium nitride light-emitting diode chip adopting the solution, achieving polarization of the light source.

Supplementary material for this article is available online

Keywords: nanoimprinting, electric-driven, flexible-roller, warped, stress-sensitive

1. Introduction

Surface nanostructures can improve the performance of optoelectronic devices by enhancing or controlling light behavior, such as emission [1–5], dynamic shaping [6–10], and detection [11–13]. Nano-patterning the surface of optoelectronic devices has attracted extensive concern [14–16]. Various nano-fabrication technologies have been attempted [17–20]. Deep ultraviolet lithography or electron-beam lithography can precisely manufacture designed nanostructures [21–24], and many high-quality optoelectronic devices have been successfully proofing [25, 26]. However, high costs or low efficiency do not apply to the large-scale manufacturing of cost-sensitive devices [27, 28]. Nanosphere lithography is cost-effective and easy to implement [29], but there is still a lack of effective means to control the self-assembly defect [30, 31]. Some limitations, such as structural dependence of

[*] Authors to whom any correspondence should be addressed.

Original content from this work may be used under the terms of the Creative Commons Attribution 4.0 licence. Any further distribution of this work must maintain attribution to the author(s) and the title of the work, journal citation and DOI.

© 2023 The Author(s). Published by IOP Publishing Ltd on behalf of the IMMT

laser interference lithography [32, 33], also characterize other methods. High performance optoelectronic devices are eagerly looking forward to large-scale nano-patterning methods.

Nanoimprint lithography (NIL) shows great potential for promoting the performance of optoelectronic devices, due to the strengths of high resolution, low-cost, and large-area preparation [34–40]. However, imprinting the designed nanostructures on the surface of an optoelectronic wafer is still challenging. To begin with, wafers are usually warped before being cut into individual devices [41, 42]. Mismatch of material and thermal properties during epitaxial growth warp the wafer's morphology [43], while epitaxial growth is indispensable [44–46]. Contact between the imprint template and wafer is hindered by the warped substrate, which destroys the prerequisite for a successful imprint [47–49]. Secondly, stress sensitivity is inherent in an optoelectronic wafer/chip [50, 51]. The external force will change the atomic distance and the effective mass of electrons, modifying the barrier of semiconductor materials [52–55]. There is a sharp contradiction between the stress-sensitive substrate and the traditional NIL technique based on mechanical pressure. In fact, higher pressure is usually loaded for an uneven substrate through the soft template to generate conformal contact [56–58], which is obviously infeasible for the optoelectronic substrate. In our previous work, step-controllable NIL is demonstrated to the uneven substrate [59], but the gas-electric cooperative control is relatively complex.

In this paper, electric-driven flexible-roller NIL (EF-NIL) is proposed, which can be adapted for the preparation of high-fidelity nanostructures on the stress-sensitive warped wafer efficiently. One end of the nanoimprint flexible template is twined around a roller with a certain distance on the substrate, which leaves the template hanging and paving on the substrate due to self-gravity. The electric field is applied to the template and the substrate. The generated electrostatic force drives the contact of the template and the substrate. When the flexible template is continuously released through the simple motion of the roller, the contact line gradually moves, driven by the electrostatic force to scan the entire substrate. The contact line may be curved for a warped wafer, but it still propagates forward, effectively avoiding bubble defects. During contact, the liquid resist completely fills the microcavities on the template jointly driven by electrostatic attraction and electro-wetting, achieving high fidelity of the fabricated structures. More important, the nanoimprint driving force, powered by electric field surface force, is not transmitted to the substrate, so the entire substrate is stress-free. In addition, the demolding process can be conveniently achieved by the roller's reverse motion. Based on EF-NIL advantages, a high-quality polarization light emitter is successfully developed by fabricating subwavelength nanogratings on the surface of flip-chips.

2. Results and discussion

The flexible template contacts with the substrate conformally, which is a prerequisite for nanoimprint process. Bubbles are easily enclosed when the template and the substrate come in face-to-face direct contact, even if the external nanoimprint pressure is present. The EF-NIL is proposed to ensure conformal adhesion between the template and substrate via the line-contact method. In this work, one side of the template was fixed on the same horizontal surface of the substrate, and the other side was conveniently entwined on a roller with a certain distance from the substrate so that the template falls on the substrate in a paving state. The template achieved continuous release and recovery through the simple movement of the roller to complete nanoimprinting. The electric field was applied to the conductive template and the substrate to provide driving force. The line contact way of the flexible-roller is characterized by reduced problems relating to trapped air bubbles, thickness variation, and dust contaminants, which greatly improves replication uniformity.

The nanoimprint process is detailed in figure 1(a-i). In the experiment, the wafer coated with liquid nanoimprint resist was placed flat on the chuck with air grooves. A pair of parallel electrodes of the substrate and the conductive template were formed when the electric field was applied. The template was released when the chuck and the roller started moving, and the side fixed to the chuck first contacted the resist. The contact front spreads forward under the electric field and device motion. Over time, the template completely contacts the entire wafer. Simultaneously, under the driving of the electric field, the microcavities on the template are also filled. The electric field was removed after a UV lamp cured the resist. Then, the chuck and the roller moved in opposite directions to peel the flexible template from the wafer. That is the peel-off demolding process, which has low strain and can use the flexibility of the template to achieve demolding on the non-flat substrates. So far, the nanoimprint process of the entire wafer was completed.

The schematic diagram of the flexible roller on the substrate is shown in figure 1(a-ii). The interface between the template and the substrate was simplified as the model shown in the inset of figure 1(a-ii), to investigate the effect of the electric field on the motion of the flexible roller. The electric field is applied on the flexible template and the substrate, driving them into conformal contact. The main driving forces F_d are the electrostatic attraction pressure F_{ea} and the electric liquid bridge force F_{eb}.

Electrostatic attraction F_{ea} is produced by the electrodes formed by the flexible template and the substrate:

$$F_{\mathrm{ea}} = \frac{\varepsilon_r^2 \varepsilon_0}{2} E^2 A \tag{1}$$

where ε_r is the average dielectric constant of the dielectric layer between the substrate and the template, ε_0 is the dielectric constant of the vacuum, and E indicates the electric field intensity.

The liquid bridge attraction F_{b} will attract the two solids when a certain amount of liquid wets the two solid surfaces between two closed solid surfaces (figure S1). F_{eb} is the

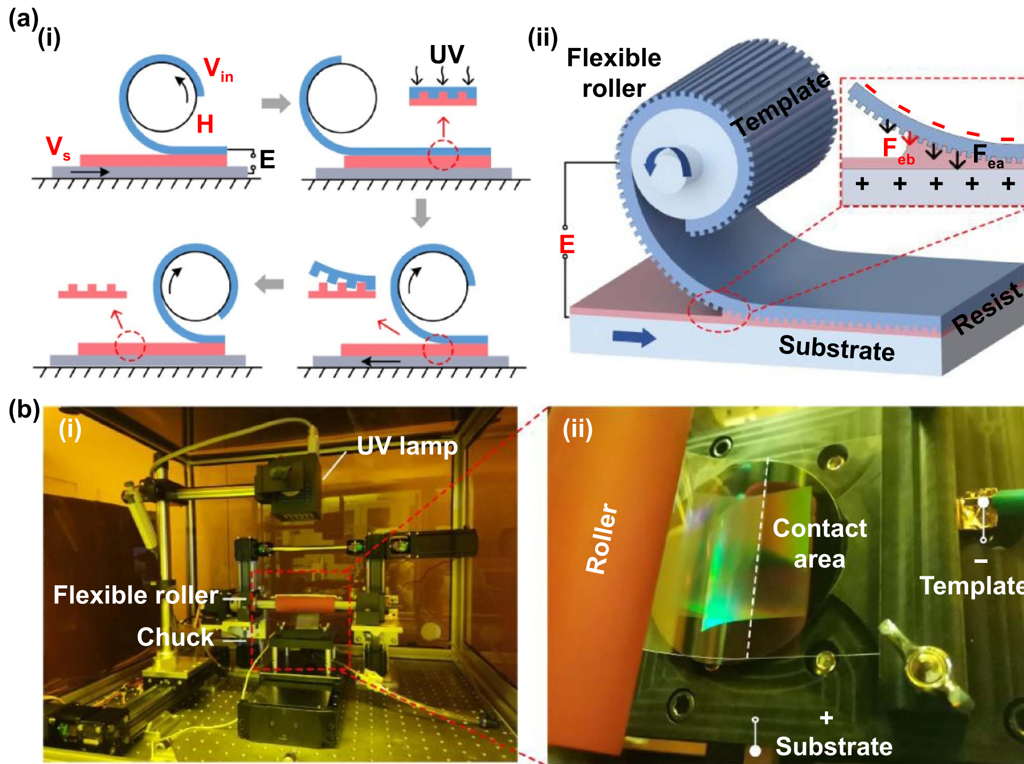

Figure 1. Schemes of the EF-NIL: (a) (i) diagram of the nanoimprint process, (ii) structural form of the flexible-roller (the inset shows a simplified model of the contact between the template and the substrate), (b) (i) EF-NIL prototype, (ii) mechanism of the electric-driven flexible-roller.

reinforcing force of F_b with electric field that can be expressed as follows:

$$F_{eb} = \frac{2\gamma A\cos\theta_E}{d} + \gamma l\sin\theta_E \quad (2)$$

where θ_E is the wetting angle after applying E, γ indicates the surface tension of the resist in air, d indicates the distance between two parallel plates, A indicates the area of two parallel solid surfaces wetted by liquid resist, and l is the circumference of the area.

A prototype machine for 4″ EF-NIL is developed based on the abovementioned principle (figure 1(b-i)). The prototype consists of a power supply, control, and motion system. The movements of the chuck, roller, UV lamp, and other modules are mainly controlled by a three-axis motion system. As the core component of the nanoimprint, the flexible conductive template consists of four layers: a backing layer, a conductive layer, a buffer layer, and a structural layer. The preparation of the flexible conductive template is detailed in the Experimental section. The mechanism of the electric-driven flexible roller is shown in figure 1(b-ii), where obvious boundaries of the contact area and the non-contact area can be seen. The spring electrode was pressed down when the wafer is fixed due to the negative pressure during nanoimprinting, so that the positive electrode can be conveniently applied to the substrate. The negative electrode is loaded on the flexible conductive template. Based on the unique advantages of the roll-based nanoimprinting technique in large area preparation, wafer-level preparation of EF-NIL technology on larger areas can be achieved with only large-size template and motion mechanisms.

Since the flexible-roller template is the scheme's core component, its motive character affects the nanoimprinting process. As shown in figure 1(a-i), the parameters that affect the movement of the template include the roller speed V_{in} (i.e. the release speed of the template), the speed of the substrate V_s, and the height of the roller on the substrate H. The diameter of the roller was set to 40 mm, and the height of the roller on the substrate was set to 50 mm to facilitate sample taking and template storage.

The driving force analysis of the template is the primary part of its movement. When no electric field is present, the driving force F_d of the template is only the liquid-bridge force F_b. In EF-NIL, the main driving forces for the template and substrate contact are the electric liquid bridge force F_{eb} and the electrostatic attraction pressure F_{ea}. F_{ea} is generated by applying the electric field, and gradually increases with the electric field intensity (figure 2(a-i)). In addition, the electric field improves the liquid-bridge force F_b to F_{eb}. The electric field greatly enhances the driving force F_d of the template paving to $E-F_d$ (the inset of figure 2(a-i)). The great driving force ensures better conformal contact between the template and the substrate. The electrostatic attraction pressure F_{ea} exists throughout the template and decreases with increased distance

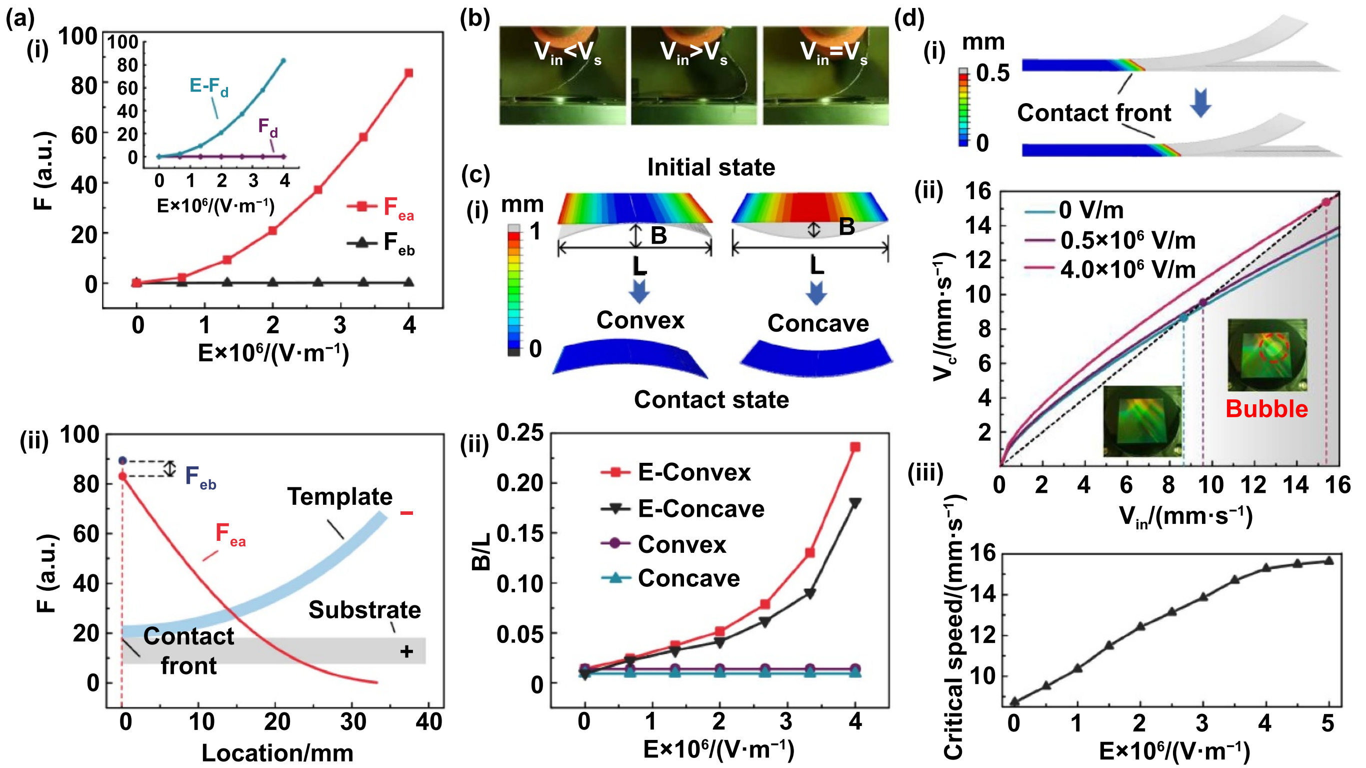

Figure 2. Effect of the electric field on the motive character of the flexible template: (a) (i) the driving force of the template, (ii) driving force of the flexible template at different positions, (b) different template forms under different relative speed between the roller and the chuck, (c) (i) simulation model of contact opening (COPEN) for flexible template adapting to warped substrate, (ii) adaptation of the template to the warped substrate at different electric field intensities, (d) (i) simulation model of COPEN for flexible template move, (ii) influence of template release speed V_{in} and intensity of the applied electric field on template paving speed V_{c}, (iii) the critical paving speed corresponding to different electric field intensities.

between two electrodes. The electric liquid bridge force F_{eb} only exists in the wetting part, that is the position of contact front. Figure 2(a-ii) shows the driving force at different positions of the template. The force on the contact line is maximal, ensuring that the template can move forward in the form of line contact and avoid the package of bubbles.

The speed of the motion mechanism affects the character of the template. Figure 2(b) shows the different flexible template forms under different relative speeds of the roller and the substrate. When $V_{\mathrm{in}} < V_{\mathrm{s}}$, the paving speed of the flexible template on the substrate is extremely slow, and the contact area is relatively small. When $V_{\mathrm{in}} > V_{\mathrm{s}}$, the flexible template is severely bent and deformed, damaging the template. When $V_{\mathrm{in}} = V_{\mathrm{s}}$, the shape of the flexible template remains in an ideal state. Therefore, the roller speed was set equal to the speed of the substrate.

The driving force provided by the electric field enables the template's good adaptability to the warped substrate, ensuring complete contact between them. The epitaxial wafer is generally characterized by concave and convex deformation due to the stress difference between different materials. Figure 2(c-i) shows a simulation model of the contact opening (COPEN) of the flexible template and the substrate. This model represents the distance of the unit nodes on the template from the substrate to explore the adaptability of the template to different warped substrates. The ratio of the warpage height and substrate length (B/L) indicates the warpage degree of the substrate. When no electric field is present, the driving force F_{d} ensures that the template adapts to the concave deformation with (B/L) is 0.0092 and convex deformation with (B/L) is 0.0138. When E is $4 \times 10^6\,\mathrm{V\,m^{-1}}$, the increased driving force ensures that the template adapts to the concave deformation with (B/L) is 0.181 and convex deformation with (B/L) is 0.236 as shown in figure 2(c-ii)). The greater the electric field intensity, the larger the warpage that can be adapted. Moreover, during the nanoimprint, the flexible composite template is generally prepared from multiple layers, usually characterized by bending deformation due to the differences in thermal stress. The electric field can also compensate for the deformation of the template to ensure complete contact, fully demonstrating the applicability of this scheme to warped substrates.

The speed of the flexible-roller directly determines the defect rate and efficiency of nanoimprinting. The conducted analysis demonstrated that the shape of the flexible template remains ideal state when the roller speed is equal to the speed of the substrate. However, air bubbles still are trapped between the template and the substrate when the roller speed is

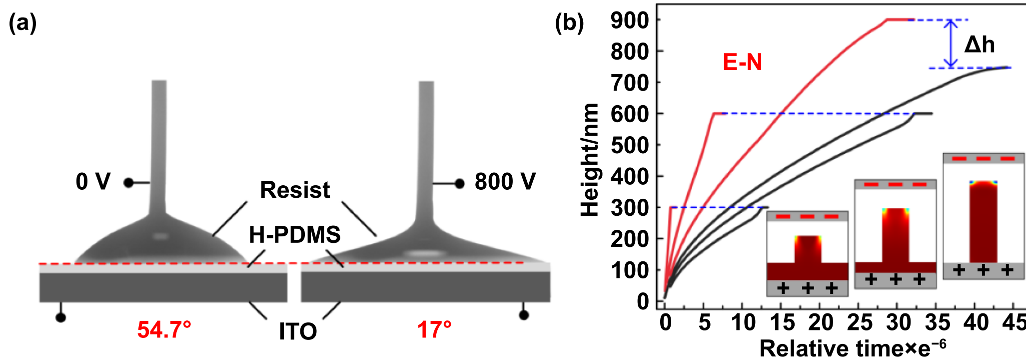

Figure 3. Effect of electric fields on structure formation: (a) resist wettability under different electric field intensities, (b) simulation renderings of nanoimprint filling structures with different aspect ratios.

extremely high. The flexible template is taken as the research object. Here, V_{in} (the speed of the roller releases template) and V_{c} (the speed of the template contact with the substrate) will affect the contact status. If $V_{\text{in}} \leqslant V_{\text{c}}$, the released template can be incompletely contact with the substrate to ensure the nanoimprint integrity. If $V_{\text{in}} \geqslant V_{\text{c}}$, the released template cannot fully contact the substrate, and air bubbles will be enclosed between the template and the substrate.

Nanoimprint efficiency increases with the release speed V_{in}, but the paving speed V_{c} does not increase proportionally with V_{in}. Therefore, the speed needs to be reasonably controlled to ensure the integrity. Furthermore, a simulation model is established to investigate the motion of the flexible-roller template under electric field (figure 2(d-i)). V_{in} was lower than V_{c} in the initial stage. V_{c} increased with V_{in}. when V_{in} reached a critical speed, V_{c} was lower than V_{in} and the wrapping bubbles (figure 2(d-ii)). V_{in} should not exceed the critical speed to ensure the integrity of the nanoimprint structures. Since the electric field increased the driving force of the template, V_{c} of the template increased, and the critical speed was also improved. The critical speed under different electric field intensities is shown in figure 2(d-iii). When no electric field was applied, the critical speed was 8.73 mm s^{-1}. When the electric field intensity (E) was $0.5 \times 10^6\,V\text{m}^{-1}$, the critical speed was 9.50 mm s^{-1}. When E is $4 \times 10^6\,V\text{m}^{-1}$, the critical speed was 15.28 mm s^{-1}, corresponding to an increase of 75.03%. This results in 42.87% reduction in the template paving time for a 4″ substrate and 24.56% reduction in the overall nanoimprint time, which contributes significantly to the efficiency of the entire nanoimprinting process.

It can be observed that an electric field increased the paving speed of the template and ensured a highly efficient nanoimprint. However, the electric field intensity is not as high as possible. The paving speed increases with the electric field intensity as shown in figure 2(d-iii)). But when E is higher than $4 \times 10^6\,V\text{m}^{-1}$, the increase is slower. On the other hand, considering the weak part during template preparation, E should not exceed $4 \times 10^6\,V\text{m}^{-1}$ to prevent the electric field breakdown of the template and causing a short circuit.

The electric field causes the template to adapt to the warped substrate, improves the nanoimprinting efficiency, and promotes the resist filling in the microcavities of the template to ensure the integrity of the forming structures. The auxo-action of the electric field on structure forming has two main factors. Firstly, the electric field can change the wetting state of the resist on the template surface, making it easier to fill the microcavities. Then, the electrostatic attraction between the two electrodes has a driving effect on the filling of the liquid resist.

Figure 3(a) shows the wettability change of the liquid resist under electric field. A 20 μm H-PDMS was spin-coated on the substrate with indium tin oxide (ITO) to simulate the actual template state, and a 5 μl resist was dropped onto the substrate. The contact angles of the resist at different voltages are shown. The wetting angle of the resist on the H-PDMS is 54.7° with no voltage, and 17° when the applied voltage is 800 V. A decrease in the contact angle increases the capillary force, causing the resist to fill microcavities more easily.

The forming process of structures was simulated with different aspect ratios based on phase field simulation to investigate the contribution of electric field to the structure formation (figure S2). The structures were set with the width of 300 nm and depths of 300 nm, 600 nm, and 900 nm, respectively, and the electric field was set to $4 \times 10^6\,V\text{m}^{-1}$. Figure 3(b) shows the variation of the rising height of the central resist surface with time in different aspect ratio structures. The red indicates the height with electric field, and the black line represents without the electric field. The structures with different aspect ratios are well formed by the electric field (the inset of figure 3(b)). The electric field can significantly reduce the resist filling time in microcavities of different heights. In addition, when the height is 900 nm, it is difficult to fill the microcavity completely by the capillary force alone (figure S2). However, the electric field can ensure the integrity of the structure. Therefore, EF-NIL can not only improve the efficiency of structure forming, but also realize the forming of structures with high aspect ratio and ensure the high fidelity of structures.

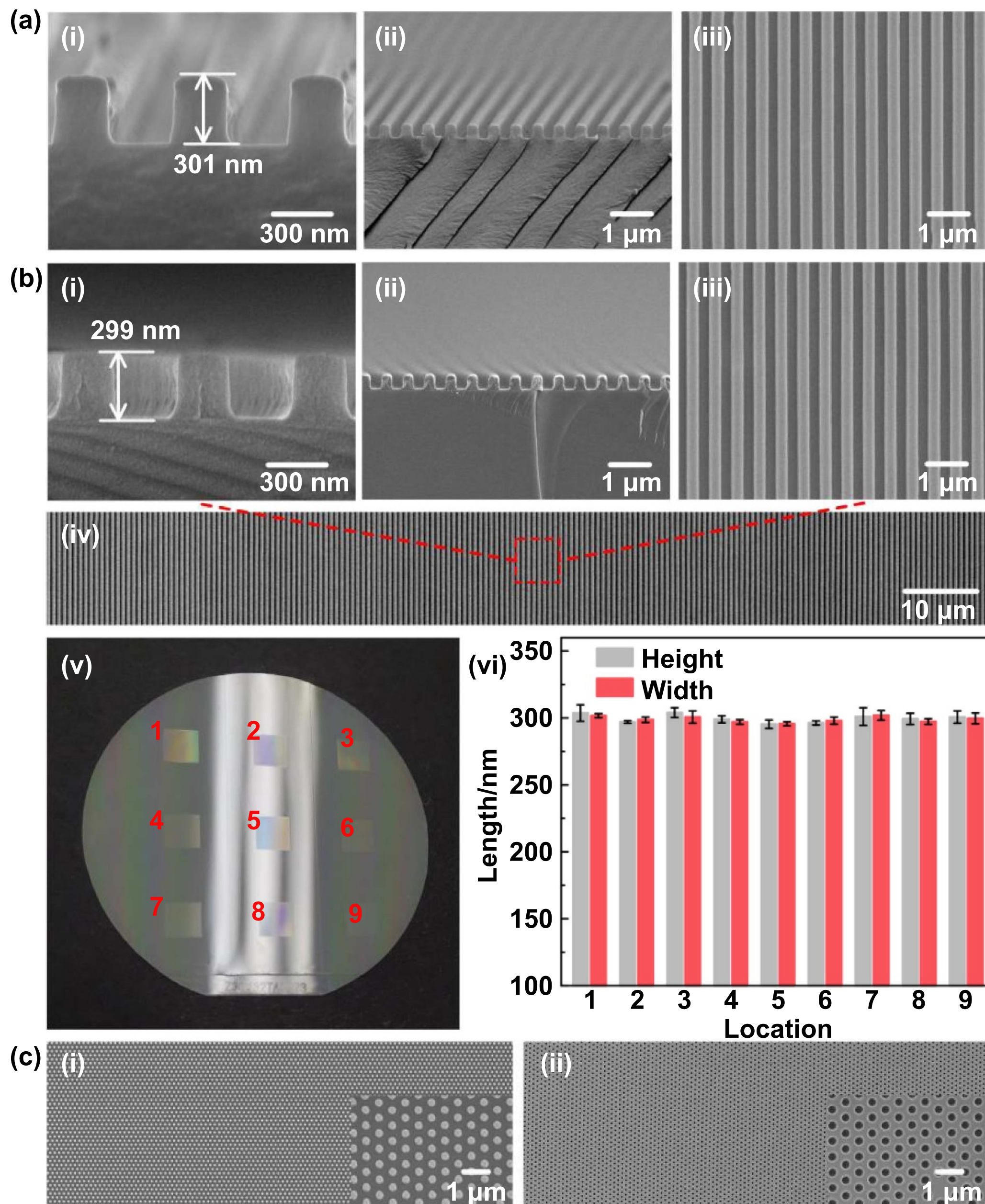

Figure 4. Structural fabrication of EF-NIL: (a) grid line array structures on the template, (b) sample and nanostructures prepared by EF-NIL, (i)–(iii) nanoimprinting structures corresponding to the template, (iv) formed structures in the large area, (v) sample containing nine nanostructured areas, (vi) height and width measurement statistics of the nanostructures in nine sample regions, (c) large area hole arrays and column arrays prepared by EF-NIL.

Nanoimprinting by a grating mold with a period of 600 nm, a line width of 300 nm, a duty ratio of 1:1, and an aspect ratio of 1:1 is shown in figure 4(a) to verify the forming capability of EF-NIL. The gallium nitride LED epitaxial wafer is used as the substrate, the thickness of the resist spin-coated on the substrate is 200 nm, and the specific experimental details of the substrate are shown in the Experimental section. The nanostructures obtained by EF-NIL on a wafer-scale GaN substrate are shown in figure 4(b). The sample images are shown in figure 4(b-v), where nine nanostructure areas are uniformly distributed, each area using the same grating structure as a template. Then, the width and height of the grating structures of nine areas were measured and counted. Three measuring points were randomly selected, and the obtained statistical chart is shown in figure 4(b-vi). In consideration of the measurement errors, the entire structure had good uniformity, because the thicknesses of both resist and structure layer of the template were homogeneous, so that the driving force generated by the two electrodes would completely cover the sample. Macroscopic and microscopic views of the grating structures

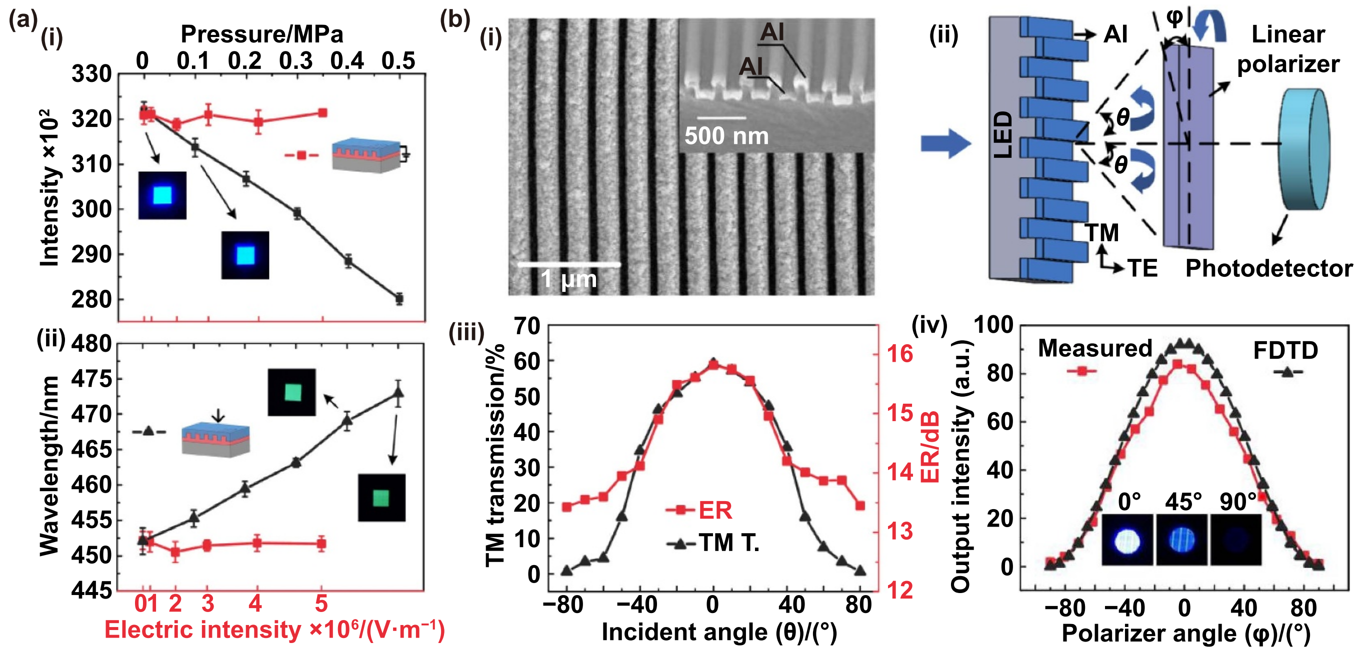

Figure 5. Polarized LED prepared by EF-NIL: (a) influence of electric field and nanoimprint force on the luminous intensity and wavelength of the chips, (b) (i) scanning electron microscope (SEM) images of the polarization gratings, (ii) diagram of the polarization measuring device, (iii) transverse magnetic (TM) transmission and extinction ratio (ER) at different incident angles when $\varphi = 0°$, (iv) light intensity obtained by experiment and simulation at different rotation angles (the inset shows the photographs of the polarized LED at rotation angles of 0°,45°, and 90°).

of the sample, respectively, are shown in figure 4(b-i-iv). It can be observed that the grating structure has a good matching degree with the template structure, indicating that the structure prepared by this scheme has high fidelity. In addition, wafer scale column arrays and hole arrays were prepared by EF-NIL (figure 4(c-i-ii)), proving the universality of the technology in preparing different shapes and aspect ratio structures with high fidelity.

The existing research on the application of nanostructures in optoelectronic devices has gradually increased from improving the most basic characteristics, such as efficiency and power level, to further developing other functional features, such as polarization emission. Taking the widely used LED chip as an example, the polarization of the light was achieved by preparing grating structures on it. The chip is composed of multilayer structures (figure S3(a)). The design of the multilayer membrane structure makes it more sensitive to stress.

Experiments were designed to validate the effect of the pressure of traditional nanoimprint and the electric field intensity of EF-NIL on device performance. Experimental details are shown in the Experimental Section, and the results are shown in figure 5(a). In EF-NIL, the luminous intensity and wavelength of the chips fluctuate within the normal range as the electric field strength increases. The driving force provided by the electric field does not affect the performance of the device. In traditional nanoimprint, a downward trend of the luminous intensity of the chip as the pressure increased. When the pressure reached 0.5 MPa, the luminous intensity dropped by 13.01%. A red shift of the emission wavelength was observed as the pressure increased, and when the pressure reached 0.5 Mpa, it was 20.83 nm. The inset of figure 5(a) shows the photographs of the chips for different pressure gradients, demonstrating that the vertical pressure had an undesirable effect on the performance of the substrate; this effect increases with the pressure.

The performance difference between the two methods can be attributed to different pressure transfer methods. The electric field acts as the surface force, and the mechanical pressure acts as the volume force (figure S3(b)). The pressure and electric intensity have a corresponding relationship for the same filling driving force as shown in figure 5(a). Compared to traditional nanoimprint, EF-NIL requires less filling driving force since the electric field can change the wettability of the resist, facilitating the filling of the cavities.

Nano-grating structures were fabricated on a flip-chip LED and its luminous peak is 450 ± 3 nm by the EF-NIL to verify the practicability of the prototype. The thickness of the resist was 200 nm, and the processing is shown in the Experimental section. During nanoimprinting, the positive of the electric field was applied to the LED top layer and the negative is applied to the conductive template.

The resist nano-grating was successfully obtained after lifting off the flexible conductive template. Following the heat evaporation of a 50 nm Al coating onto the resist nano-grating, the polarized nano-grating was created. Figure 5(b-i) shows the SEM pictures of the planform and the cross-sectional image of the nano-grating. The images demonstrated that the composite nano-grating had a period of 200 nm, a line width of 100 nm, a duty ratio of 1:1, and a height of 200 nm. Moreover, the thickness of the metal layer was 50 nm since polarization grating can achieve a strong TM transmission and extinction

ratio (ER) at this thickness, as analyzed by the finite difference time domain (FDTD) simulation (figure S4(b)).

To explore the polarization capability of the emitter, its intensity of the photoluminescence (PL) spectra of polarized TM and transverse elelctric (TE) light was tested using the measuring device in figure 5(b-ii). A steady transient fluorescence spectrometer was employed in the experimental setup to provide excitation light and collect luminance. Moreover, a linear polarizer purchased from Edmund Optics was used to detect the polarization effect.

The TM transmission and ERs of the chip at different incident angles are shown in figure 5(b-iii)). The 0° direction means that the incident light is perpendicular to the LED, after which we test every 10 degrees in the −80°–80°. In the 0° direction, TM transmittance was highest, and TE transmittance was lowest, so the highest ER was 15.85. The efficient period of the grating changed with the incident angle. Simultaneously, the TM transmission and ER of the chip decreased. The light intensity significantly dropped as the linear polarizer was rotated by 90° as shown in figure 5(b-iv)), showing that the LED chip has ideal polarization capability. Photographs of the polarized emitter after rotating the linear polarizer in three different angles of $\theta = 0°$, 45°, and 90° are shown in the inset. This figure also shows the FDTD simulation results of the subwavelength grating, which fit in well with the experimental results.

The optimized design of the structure is particularly important for improving the performance of the LED chip. The accuracy of the grating structure plays a crucial role in the chip's performance (figure S4(a)). The focus of this application program is to verify the feasibility of the EF-NIL in preparing nanostructures on stress-sensitive semiconductor substrates, so that the selected template in this solution is ready-made. A better polarization effect can be achieved if the structural design is optimized in detail.

3. Experimental section

3.1. Preparation of flexible transparent conductive template

The manufacturing process of the flexible conductive template is demonstrated detailed in figure 6. The template can be prepared by the prototype machine. The 50 μm polyethylene terephthalate (PET) film was used as the backing of the template due to its transparency and flexibility. To begin with, the 100 nm indium tin oxide (ITO) was sputtered by Denton Vacuum Discovery 635 equipment as electrode on the PET, which has good conductivity with sheet resistance is 8 Ω sq^{-1}. It is transparent and does not prevent the transmission of UV light during the curing process. Then, sputtering 50 nm SiO2 coating as the adhesive layer between the electrode and the buffer layer on the back of the electrode (figure 6(a)). The H-PDMS was used to prepare the structural layer with its high resolution and low shrinkage. A thin layer of liquid H-PDMS with a thickness of about 20 μm was spin-coated on the silicon template with nanostructures (figure 6(b)). Then, 180 μm PDMS (Sylgard® 184, Sigma-Aldrich) was spin-coated as the buffer layer (figure 6(c)). Next, the backplane PET layer with transparent electrodes was bonded to the PDMS layer in the prototype machine (figure 6(d)). PDMS was cured at 85 °C for 20 min. Finally, the flexible transparent conductive template was peeled off from the mold (figure 6(e)).

3.2. Experiments on GaN Wafer

In the experiment, the LED chip and the epi-wafers were purchased from Yangzhou Zhongke Semiconductor Lighting Co. Ltd Before the experiment, the substrates were baked at 200 °C for 30 min to remove moisture and impurities on the surface and cooled to room temperature immediately. The wafers were spin coated with 8 nm mr-APS1 polymer as adhesion layer at 5000 rpm for 60 s, and baked on a hot plate at 150 °C for 60 s to remove the solvent. Then, the 200 nm mr-UVcur21 polymer was spin-coated on the substrate at 3000 rpm for 60 s, and baked at 80 °C for 60 s on a hot plate before UV exposure. The mr-APS1 adhesion promoter and the mr-UVcur21 UV-curable polymer were purchased from Micro Resist Technology, GmbH. The resist had low viscosity and high curing rate designed for UV-based NIL.

3.3. Experiments on the influence of different pressure and electric field intensity on the substrate performance

The LED chip with a peak wavelength of 450 ± 3 nm prepared by flip-chip technology was chose as the substrate. In EF-NIL, we set up a gradient of six different electric field intensities of 0, 1×10^6, 2×10^6, 3×10^6, 4×10^6, and $5 \times 10^6\ V\mathrm{m}^{-1}$ to study the influence of the electric field on the chip, and eight samples were tested for each electric field intensity. The electric field was applied to the conductive template and the substrate for 60 s. After the test is completed, the changes in the emission wavelength and intensity of the chip under different electric field gradients were analyzed by PL spectrometry using the steady transient fluorescence spectrometer (QM-400), with the gap width of which is 2 mm, and the excitation wavelength of 467 nm. Finally, we averaged the test parameters of the eight samples for each electric field gradient. Correspondingly, in mechanical nanoimprint, the influence of the vertical pressure on the substrate is simulated by the tension testing machine PT-1198GDP. The area of the indenter was larger than the chip area to ensure that the chip is fully compressed for 60 s to simulate the actual nanoimprint. In this work, seven sets of pressure gradients of 0, 0.1, 0.2, 0.3, 0.4, and 0.5 MPa were tested with eight samples. The emission wavelength and intensity were tested by the same test method and under the test conditions as in the above experiments.

3.4. Characterization

The SEM pictures are taken through the Hitachi S-3000N SEM. The wetting angle is tested by an OCA15EC (Data Physics).

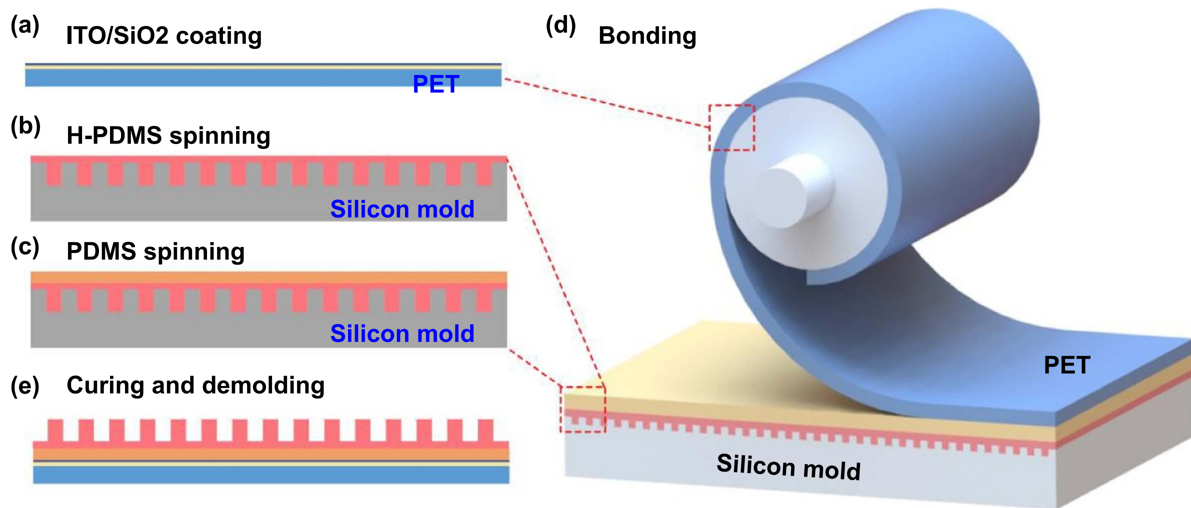

Figure 6. Preparation process of the flexible conductive template: (a) preparation of the conductive layer on the PET, (b) preparation of the structural layer, (c) preparation of the buffer layer, (d) bonding the backing layer, buffer layer and the structural layer, (e) curing and demolding.

4. Conclusion

In this paper, EF-NIL was proposed, which achieves wafer-scale high-fidelity nanoimprint on stress-sensitive warpage substrates. The proposed method employs a continuously released and recovered flexible conductive template in the form of a flexible roller by controlling the roller's movement. The electric field between the template and the substrate provides the driving force. Under the electric field, the line contact of the flexible roller can adapt to the warped substrate, and ensure the conformal adhesion of the template and substrate. The electric field force does not transfer to the substrate as a surface force. Hence, the substrate is free from external force. In addition, the fidelity and uniformity of the structures are also guaranteed with the action of electric field. Nanograting structures are fabricated on a 4 in. GaN chip with high fidelity using the proposed process and prototype to polarize the LED chip directly. The proposed method provides a technical solution for fabricating nanostructures on stress-sensitive warped substrates in biology, precision optical elements, high-efficiency solar cells and other important fields.

Acknowledgments

This work is financed by the National Natural Science Foundation of China (Nos. 52025055 and 5227050783).

ORCID iD

Jinyou Shao https://orcid.org/0000-0003-2525-4587

References

[1] Joo W J *et al* 2020 Metasurface-driven OLED displays beyond 10,000 pixels per inch *Science* **370** 459–63
[2] Xu L H, Ou Q D, Li Y Q, Zhang Y B, Zhao X D, Xiang H Y, Chen J D, Zhou L, Lee S T and Tang J X 2016 Microcavity-free broadband light outcoupling enhancement in flexible organic light-emitting diodes with nanostructured transparent metal–dielectric composite electrodes *ACS Nano* **10** 1625–32
[3] Pourdavoud N, Wang S, Mayer A, Hu T, Chen Y W, Marianovich A, Kowalsky W, Heiderhoff R, Scheer H C and Riedl T 2017 Photonic nanostructures patterned by thermal nanoimprint directly into organo-metal halide perovskites *Adv. Mater.* **29** 1605003
[4] Wang C H, Fan Y, Shao J Y, Yang Z J, Sun J X, Tian H M and Li X M 2021 Discretely-supported nanoimprint lithography for patterning the high-spatial-frequency stepped surface *Nano Res.* **14** 2606–12
[5] Cao T, Lian M, Liu K, Lou X C, Guo Y M and Guo D M 2022 Wideband mid-infrared thermal emitter based on stacked nanocavity metasurfaces *Int. J. Extrem. Manuf.* **4** 015402
[6] Li P N, Dolado I, Alfaro-Mozaz F J, Casanova F, Hueso L E, Liu S, Edgar J H, Nikitin A Y, Vélez S and Hillenbrand R 2018 Infrared hyperbolic metasurface based on nanostructured van der Waals materials *Science* **359** 892–6
[7] Kuznetsov A I, Miroshnichenko A E, Brongersma M L, Kivshar Y S and Luk'Yanchuk B 2016 Optically resonant dielectric nanostructures *Science* **354** aag2472
[8] Wang C H, Lai D S, Fan Y, Tian H M, Li X M, Chen X L and Shao J Y 2021 Nanoimprinting metal-containing nanoparticle-doped gratings to enhance the polarization of light-emitting chips by induced scattering *Nanotechnology* **32** 235304
[9] Wu G B, Zhu S Y, Pang S W and Chan C H 2022 Superheterodyne-inspired waveguide-integrated metasurfaces for flexible free-space light manipulation *Nanophotonics* **11** 4499–514
[10] Feng B, Chen Y F, Sun D, Yang Z Y, Yang B, Li X and Li T 2021 Precision integration of grating-based polarizers onto focal plane arrays of near-infrared photovoltaic detectors for enhanced contrast polarimetric imaging *Int. J. Extrem. Manuf.* **3** 035201
[11] Tian W, Liu D, Cao F R and Li L 2017 Hybrid nanostructures for photodetectors *Adv. Opt. Mater.* **5** 1600468
[12] Oh D K, Lee T, Ko B, Badloe T, Ok J G and Rho J 2021 Nanoimprint lithography for high-throughput fabrication of metasurfaces *Front. Optoelectron.* **14** 229–51

[13] Zhu S Y, Wu G B, Pang S W and Chan C H 2022 Compact terahertz dielectric folded metasurface *Adv. Opt. Mater.* **10** 2101663
[14] Zhou P L, Yu H B, Zhong Y, Zou W H, Wang Z D and Liu L Q 2020 Fabrication of waterproof artificial compound eyes with variable field of view based on the bioinspiration from natural hierarchical micro–nanostructures *Nano-Micro Lett.* **12** 166
[15] Ji D Y, Li T and Fuchs H 2020 Patterning and applications of nanoporous structures in organic electronics *Nano Today* **31** 100843
[16] So S and Rho J 2019 Designing nanophotonic structures using conditional deep convolutional generative adversarial networks *Nanophotonics* **8** 1255–61
[17] Ma Z B, Jiang C Y, Yuan W Z and He Y 2013 Large-scale patterning of hydrophobic silicon nanostructure arrays fabricated by dual lithography and deep reactive ion etching *Nano-Micro Lett.* **5** 7–12
[18] Lee Y H, Lee T K, Song I, Yu H, Lee J, Ko H, Kwak S K and Oh J H 2016 Boosting the performance of organic optoelectronic devices using multiple-patterned plasmonic nanostructures *Adv. Mater.* **28** 4976–82
[19] Willson C G and Roman B J 2008 The future of lithography: SEMATECH Litho Forum 2008 *ACS Nano* **2** 1323–8
[20] Chen Y Q, Shu Z W, Zhang S, Zeng P, Liang H K, Zheng M J and Duan H G 2021 Sub-10 nm fabrication: methods and applications *Int. J. Extrem. Manuf.* **3** 032002
[21] Totzeck M, Ulrich W, Göhnermeier A and Kaiser W 2007 Pushing deep ultraviolet lithography to its limits *Nat. Photon.* **1** 629–31
[22] Zhu X L, Czolkos I, Johansson A, Nielsen T and Kristensen A 2021 Master origination by 248 nm DUV lithography for plasmonic color generation *Appl. Phys. Lett.* **118** 141103
[23] Thomas J 2007 Body sculpting *Nat. Nanotechnol.* **2**
[24] Yong J L, Yang Q, Huo J L, Hou X and Chen F 2022 Underwater gas self-transportation along femtosecond laser-written open superhydrophobic surface microchannels ($<$100 μm) for bubble/gas manipulation *Int. J. Extrem. Manuf.* **4** 015002
[25] Wierer J J Jr, David A and Megens M M 2009 III-nitride photonic-crystal light-emitting diodes with high extraction efficiency *Nat. Photon.* **3** 163–9
[26] Leung S F, Zhang Q P, Xiu F, Yu D L, Ho J C, Li D D and Fan Z Y 2014 Light management with nanostructures for optoelectronic devices *J. Phys. Chem. Lett.* **5** 1479–95
[27] Kim S, Hyun S, Lee J, Lee K S, Lee W and Kim J K 2018 Anodized aluminum oxide/polydimethylsiloxane hybrid mold for roll-to-roll nanoimprinting *Adv. Funct. Mater.* **28** 1800197
[28] Cai Y J, Qin A J and Tang B Z 2017 Siloles in optoelectronic devices *J. Mater. Chem.* C **5** 7375–89
[29] Huang X H and Li T 2020 Recent progress in the development of molecular-scale electronics based on photoswitchable molecules *J. Mater. Chem.* C **8** 821–48
[30] Zhang J H, Li Y F, Zhang X M and Yang B 2010 Colloidal self-assembly meets nanofabrication: from two-dimensional colloidal crystals to nanostructure arrays *Adv. Mater.* **22** 4249–69
[31] Li J, Hu Y X, Yu L, Li L, Ji D Y, Li L Q, Hu W P and Fuchs H 2021 Recent advances of nanospheres lithography in organic electronics *Small* **17** 2100724
[32] Weber D, Heimburger R, Hildebrand D, Junghans T, Schondelmaier G, Walther C and Schondelmaier D 2019 Use of beam-shaping optics for wafer-scaled nanopatterning in laser interference lithography *Appl. Phys.* A **125** 307
[33] Wu J, Geng Z X, Xie Y Y, Fan Z Y, Su Y, Xu C and Chen H D 2019 The fabrication of nanostructures on polydimethylsiloxane by laser interference lithography *Nanomaterials* **9** 73
[34] Cai S X, Sun Y L, Chu H H, Yang W G, Yu H B and Liu L Q 2021 Microlenses arrays: fabrication, materials, and applications *Microsc. Res. Tech.* **84** 2784–806
[35] Ahn S H and Guo L J 2009 Large-area roll-to-roll and roll-to-plate nanoimprint lithography: a step toward high-throughput application of continuous nanoimprinting *ACS Nano* **3** 2304–10
[36] Leitgeb M, Nees D, Ruttloff S, Palfinger U, Götz J, Liska R, Belegratis M R and Stadlober B 2016 Multilength scale patterning of functional layers by roll-to-roll ultraviolet-light-assisted nanoimprint lithography *ACS Nano* **10** 4926–41
[37] Jeong B, Han H, Kim H H, Choi W K, Park Y J and Park C 2020 Polymer-assisted nanoimprinting for environment- and phase-stable perovskite nanopatterns *ACS Nano* **14** 1645–55
[38] Zhao Z J *et al* 2021 Large-area nanogap-controlled 3D nanoarchitectures fabricated via layer-by-layer nanoimprint *ACS Nano* **15** 503–14
[39] Sreenivasan S V 2017 Nanoimprint lithography steppers for volume fabrication of leading-edge semiconductor integrated circuits *Microsyst. Nanoeng.* **3** 17075
[40] Palmieri F, Adams J, Long B, Heath W, Tsiartas P and Willson C G 2007 Design of reversible cross-linkers for step and flash imprint lithography imprint resists *ACS Nano* **1** 307–12
[41] Wang Z, Zhu S J, Shan X Y, Yuan Z X, Cui X G and Tian P F 2021 Full-color micro-LED display based on a single chip with two types of InGaN/GaN MQWs *Opt. Lett.* **46** 4358–61
[42] Zhang H *et al* 2022 Monolithic GaN optoelectronic system on a Si substrate *Appl. Phys. Lett.* **121** 181103
[43] Chen W X, Hu X H, Ni Z B, Han T Q and Lu X F 2016 State of strain in GaN material as derived by optical feedback measurement *Optik* **127** 3976–8
[44] Tan C L, Chen J Z, Wu X J and Zhang H 2018 Epitaxial growth of hybrid nanostructures *Nat. Rev. Mater.* **3** 17089
[45] Martin-Bragado I and Sarikov A 2016 Atomistic modeling of epitaxial growth of semiconductor materials *Mater. Sci. Semicond. Process.* **42** 223–9
[46] Chen F R *et al* 2022 Mass transfer techniques for large-scale and high-density microLED arrays *Int. J. Extrem. Manuf.* **4** 042005
[47] Guo L J 2007 Nanoimprint lithography: methods and material requirements *Adv. Mater.* **19** 495–513
[48] Schmitt H, Duempelmann P, Fader R, Rommel M, Bauer A J, Frey L, Brehm M and Kraft A 2012 Life time evaluation of PDMS stamps for UV-enhanced substrate conformal imprint lithography *Microelectron. Eng.* **98** 275–8
[49] Hu X, Wang H Q, Zhai C, Ge H X and Cui Y S 2016 Fabrication of metallic patterns on highly curved substrates *via* nanoimprint lithography in association with an etch-in process *J. Mater. Chem.* C **4** 11104–9
[50] Wang C H, Shao J Y, Lai D S, Tian H M and Li X M 2019 Suspended-template electric-assisted nanoimprinting for hierarchical micro-nanostructures on a fragile substrate *ACS Nano* **13** 10333–42
[51] Zhao S Y, Song Y X, Liang H, Jin T T, Lin J J, Yue L, You T G, Wang C, Ou X and Wang S M 2020 Stress and strain analysis of Si-based III–V template fabricated by ion-slicing *Chin. Phys.* B **29** 077303
[52] Ben J W *et al* 2019 Influence of dislocations on the refractive index of AlN by nanoscale strain field *Nanoscale Res. Lett.* **14** 184

[53] Myers D R 1991 Issues in the realization of strained-layer quantum well optoelectronic devices *Opt. Quant. Electron.* **23** S985–94
[54] Song J, Ding Z, Liu X F, Huang Z C, Li J W, Wei J M, Luo Z J, Wang J H and Guo X 2021 The effect of biaxial tensile strain on structure and photoelectric properties of Fe-doped GaN monolayer *Comput. Mater. Sci.* **197** 110644
[55] Fu X W, Nie H X, Sun Z P, Feng M, Chen X, Liu C, Liu F, Yu D P and Liao Z M 2022 Bending strain effects on the optical and optoelectric properties of GaN nanowires *Nano Res.* **15** 4575–81
[56] Sonne M R, Smistrup K, Hannibal M, Thorborg J, Nørregaard J and Hattel J H 2015 Modeling and simulation of the deformation process of PTFE flexible stamps for nanoimprint lithography on curved surfaces *J. Mater. Process. Technol.* **216** 418–29
[57] Jeon S *et al* 2021 Rotating cylinder-assisted nanoimprint lithography for enhanced chemisorbable filtration complemented by molecularly imprinted polymers *Small* **17** 2105733
[58] Dickson M N, Tsao J, Liang E I, Navarro N I, Patel Y R and Yee A F 2017 Conformal reversal imprint lithography for polymer nanostructuring over large curved geometries *J. Vac. Sci. Technol.* B **35** 021602
[59] Wang C H, Shao J Y, Tian H M, Li X M, Ding Y C and Li B Q 2016 Step-controllable electric-field-assisted nanoimprint lithography for uneven large-area substrates *ACS Nano* **10** 4354–63